Published online 2 March 2023

Nucleic Acids Research, 2023, Vol. 51, No. 6 ***2891–2903***
https://doi.org/10.1093/nar/gkad110

Tuning strand displacement kinetics enables programmable ZTP riboswitch dynamic range *in vivo*

David Z. Bushhouse [1,2] and Julius B. Lucks [1,2,3,4,5,6,*]

[1]Interdisciplinary Biological Sciences Graduate Program, Northwestern University, Evanston, IL 60208, USA, [2]Center for Synthetic Biology, Northwestern University, Evanston, IL 60208, USA, [3]Department of Chemical and Biological Engineering, Northwestern University, Evanston, IL 60208, USA, [4]Center for Water Research, Northwestern University, Evanston, IL 60208, USA, [5]Center for Engineering Sustainability and Resilience, Northwestern University, Evanston, IL 60208, USA and [6]International Institute for Nanotechnology, Northwestern University, Evanston, IL 60208, USA

Received October 20, 2022; Revised January 20, 2023; Editorial Decision February 02, 2023; Accepted February 07, 2023

ABSTRACT

A large body of work has shown that transcriptional riboswitches function through internal strand displacement mechanisms that guide the formation of alternative structures which drive regulatory outcomes. Here, we sought to investigate this phenomenon using the *Clostridium beijerinckii pfl* ZTP riboswitch as a model system. Using functional mutagenesis with *Escherichia coli* gene expression assays, we show that mutations designed to slow strand displacement of the expression platform enable precise tuning of riboswitch dynamic range (2.4–34-fold), depending on the type of kinetic barrier introduced, and the position of the barrier relative to the strand displacement nucleation site. We also show that expression platforms from a range of different *Clostridium* ZTP riboswitches contain sequences that impose these barriers to affect dynamic range in these different contexts. Finally, we use sequence design to flip the regulatory logic of the riboswitch to create a transcriptional OFF-switch, and show that the same barriers to strand displacement tune dynamic range in this synthetic context. Together, our findings further elucidate how strand displacement can be manipulated to alter the riboswitch decision landscape, suggesting that this could be a mechanism by which evolution tunes riboswitch sequence, and providing an approach to optimize synthetic riboswitches for biotechnology applications.

GRAPHICAL ABSTRACT

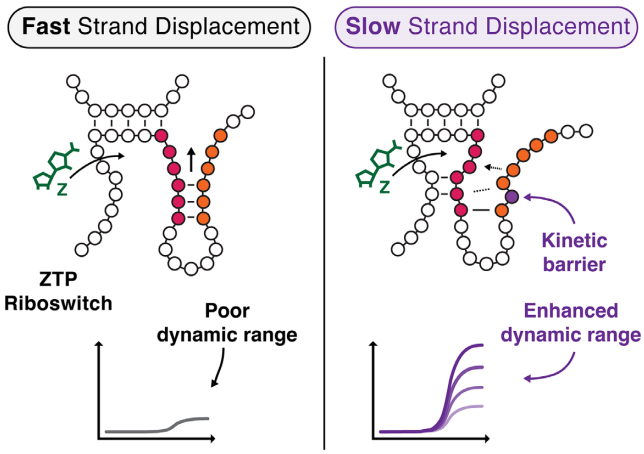

INTRODUCTION

Riboswitches are an ancient and diverse class of non-coding RNAs that regulate the expression of downstream genes in response to small molecule ligands (1). Riboswitches typically comprise an upstream highly conserved ligand-binding aptamer domain (AD) coupled to an expression platform (EP) that senses AD binding state and executes a gene-regulatory decision in response (1). Over the past 20 years, considerable progress has been made in understanding AD-ligand interactions, with high-resolution structures of riboswitch ADs revealing diverse and intricate ligand-binding architectures (2–4). In addition, bioinformatic analyses have been used to accurately predict the folding pathways and final structures of ADs using sequence conservation and covariation analysis (5,6). However, the same bioinformatic analysis is more difficult for EPs because of poor sequence conservation; across evolutionary distances, highly conserved ADs are often coupled with completely different EPs to achieve different modes of gene

*To whom correspondence should be addressed. Tel: +1 847 467 2943; Email: jblucks@northwestern.edu

regulation (7). In general, EPs sense AD-ligand binding states and convert that information into a gene expression decision through EP structural switching mechanisms that are actively being investigated.

Ligand sensing and switching pose particularly difficult challenges for intrinsic transcriptional riboswitches, which execute their genetic decision during active transcription. The constraint that their genetic decision must be made in a short time window necessitates that they bind ligand cotranscriptionally, which in turn means that the folding of their EP into either an intrinsic terminator or anti-terminator structure must occur within the ms-s timescale of transcription (8). Early work demonstrated that transcriptional riboswitch function is highly dependent upon the rate of transcription (NTP concentration) and transcriptional dynamics (RNAP pausing) (9), but mechanistic details of how EPs fold during the kinetic regime of transcription have been harder to decipher. Recent advances applying diverse biophysical techniques and RNA structure chemical probing methods are beginning to uncover some of these cotranscriptional EP folding mechanisms (10–16). Collectively, these studies are starting to show that many transcriptional riboswitches perform rapid decision-making between two mutually exclusive EP structural states via internal strand displacement mechanisms.

Strand displacement is a conformational switching process in which a substrate duplex of nucleic acids is disrupted by a third invader strand, resulting in a new duplex that contains the invader and one of the original substrate strands (17). This process has been long-appreciated as a mechanism that allows RNA structures with similar free energies to quickly interconvert between each other (18). Recent work is showing that strand displacement is a critical component of transcriptional riboswitch mechanisms. For example, in the fluoride riboswitch a strand displacement process is required to form a terminator hairpin, while fluoride binding stabilizes tertiary interactions that block strand displacement, turning gene expression ON (16). In the case of the purine riboswitch *yxjA*, ligand binding blocks the strand displacement-mediated formation of an anti-terminator hairpin, turning gene expression OFF (11). In both of these riboswitches, a key strand displacement reaction both senses AD-ligand binding state and, in the absence of ligand, initiates the structural rearrangements necessary to make the corresponding gene expression decision.

Strand displacement has also been widely studied within the field of nucleic acid nanotechnology, where detailed measurements of strand displacement kinetics have been used to uncover sequence and structural features that promote and inhibit the process. For example, mismatches between the invading and substrate strands have been shown to modulate strand displacement reaction kinetics over three orders of magnitude (19–23). The ability to precisely tune strand displacement kinetics has in turn been used to manipulate the function of synthetic nucleic acid systems that utilize strand displacement. For example, mismatches have been applied to substantially decrease leak in catalytic hairpin assembly circuits (24), to bias against undesired strand displacement reactions in complex temporal logic circuits (25), and to enable high fidelity detection of mutations in single-nucleotide-specific programmable riboregulators (26).

The precision with which strand displacement systems can be manipulated, and the fact that a number of transcriptional riboswitches have been shown to utilize strand displacement, together motivate the intriguing hypothesis that riboswitch function can be tuned through EP sequence changes that alter strand displacement kinetics. Here we investigate this hypothesis through systematic studies of the ZTP riboswitch, a model transcriptional ON-switch that has been shown to use strand displacement for its switching mechanism. The ZTP riboswitch senses the metabolic intermediate 5-aminoimidazole–4–carboxamide ribonucleotide (Z) and phosphorylated analogs as indicators of folate stress (27). The highly conserved AD of this riboswitch features a 5' helix-junction-helix motif (P1-J1/2-P2) and a short 3' stemloop (P3) connected by a variable linker sequence and an H-type pseudoknot (PK) (Figure 1A) (4,28,29). During transcription in the absence of ligand, a nascent 3' portion of the EP denoted the invading domain (called 'invader' throughout) disrupts the apo-AD, resulting in the formation of a strong intrinsic terminator hairpin EP fold; however, in the presence of Z, ligand-dependent stabilizations of the AD prevent disruption by the invader, forcing the EP to follow an alternative folding pathway and allowing RNAP to escape the termination site (Figure 1A) (15,27). Thus, the EP folding pathway both senses AD:ligand binding state and commits to a gene expression outcome based on a single attempted conformational switch: disruption of the AD by the invader (Figure 1A) (13,15,30).

Previous work with the *Clostridium beijerinckii* (*Cbe*) *pfl* ZTP riboswitch showed that the disruption of the AD in the absence of Z proceeds via a strand displacement mechanism (15), which has been supported by later smFRET and NMR studies of the *Fusobacterium ulcerans* and *Thermosinus carboxydivorans* ZTP riboswitches, respectively (13,30). Building off of this work, we used a functional mutagenesis approach with *Escherichia coli in vivo* reporter assays to show that kinetic barriers to strand displacement can be used to tune ZTP riboswitch dynamic range. We first developed an *E. coli in vivo* reporter assay to measure riboswitch function, and subsequently identified EP sequence and structure features that modulate riboswitch dynamic range by tuning the favorability of strand displacement. We next investigated naturally occurring ZTP riboswitch EPs from different organisms. Testing these EP variants in our expression context showed that this strand displacement tuning strategy may be employed across *Clostridium* to achieve a variety of expression levels in different regulatory contexts. To gain a deeper understanding of how tuning strand displacement kinetics affects ZTP riboswitch dynamic range, we performed a systematic study of EP variants and found a quantitative relationship between the type and position of mutations and observed dynamic range. This understanding allowed us to create ZTP riboswitch variants with programmable dynamic range from 2.2 to 34 fold. As a final step, we synthetically flipped the logic of the *Cbe pfl* ZTP riboswitch by adding a competing strand displacement process, and showed that the same kinetic barriers to strand displacement improve dynamic range in this novel context. Together, our findings further elucidate how strand displace-

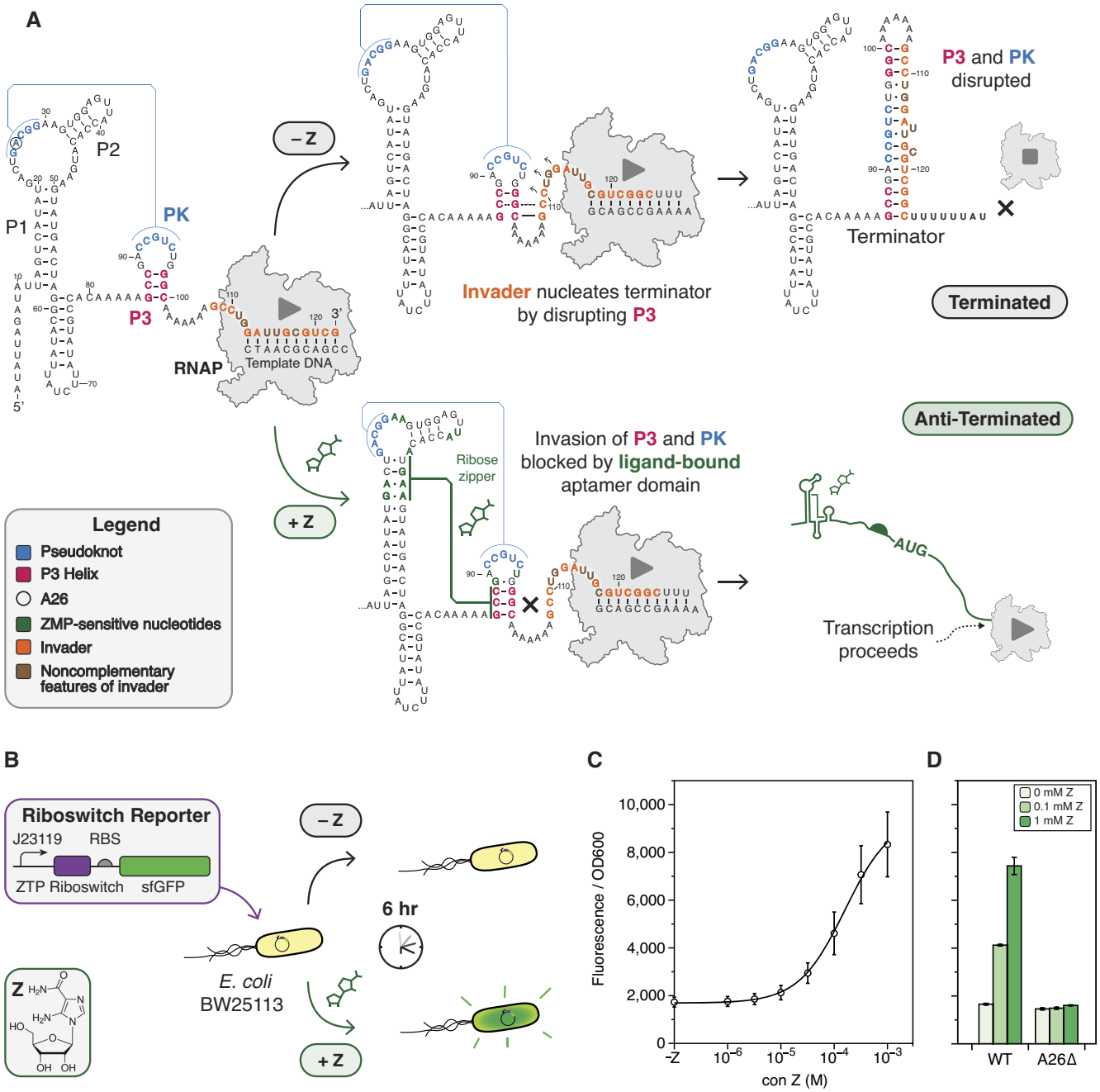

Figure 1. Development of a cellular assay for riboswitch functional mutagenesis. (**A**) Folding pathway of the *Cbe pfl* ZTP riboswitch highlighting key ligand-dependent structural transitions. In the absence of ligand, the aptamer P3 stem (red) and pseudoknot (PK, blue) are disrupted by the invader (orange) of the expression platform via a strand displacement mechanism, forming a terminator hairpin that attenuates transcription. In the presence of Z (green), the aptamer is stabilized by a ligand-dependent hydrogen bonding network that blocks strand displacement, leading to the formation of a non-attenuating alternative structure by the invader. The folding pathway was modeled from cotranscriptional SHAPE experiments (15), with nucleotides shown to have altered SHAPE reactivity in the presence of ZMP colored in green. (**B**) A schematic of the cellular assay used in this work and modified from a similar approach by Kim et al. (27). (**C**) Dose-response of the wildtype *Cbe pfl* ZTP riboswitch expression construct in *E. coli* with the indicated concentrations of Z supplied to the growth media. (**D**) A limited dose response of the WT construct and the A26Δ mutation (circled in (A)). Deletion of A26 results in a broken OFF phenotype that no longer responds to Z (y-axis as in (C)). Points (C) and bars (D) represent averages from three experimental replicates, each performed with triplicate biological replicates for a total of nine data points (n = 9), with error bars representing standard deviation.

ment can be manipulated to alter riboswitch dynamic range, suggesting that this could be a mechanism by which evolution tunes riboswitch decision-landscapes, and providing an approach to optimize synthetic riboswitches for biotechnology applications.

MATERIALS AND METHODS

Cloning and plasmid construction

Each riboswitch reporter plasmid was constructed by inserting the *C. beijerinckii pfl* ZTP riboswitch sequence downstream of the J23119 *E. coli* σ^{70} consensus promoter and upstream of a ribosome binding site and the coding sequence for superfolder green fluorescent protein (sfGFP) in a p15A plasmid backbone with chloramphenicol resistance. Riboswitch mutants were generated by inverse polymerase chain reaction (iPCR) using primers ordered from Integrated DNA Technologies (IDT). Using New England Biosciences (NEB) Phusion® High-Fidelity PCR Kit, 50μl PCRs were assembled with 1–10 ng/μl DNA template, 200 μM dNTPs (NEB), 1X Phusion® HF Buffer, 400 nM each of forward and reverse primers, and 0.25 μl Phusion® polymerase (2000 U/ml). iPCR products were run on 1% agarose gels to confirm amplification of the desired length products. 0.25 μl DpnI (NEB) was used to digest background plasmid, and PCR cleanup was performed with buffers from the QIAquick PCR Purification Kit (Qiagen) using EconoSpin® All-in-One mini spin columns (Epoch Life Science). Eluted DNA was used to assemble phosphorylation-ligation reactions with 1× T4 DNA Ligase Buffer (NEB), 0.25 μl T4 PNK (NEB), and 0.25 μl T4 DNA ligase (NEB). Ligated products were used to transform NEBTurbo® chemically competent cells, which were recovered in a benchtop shaker at 1000 rpm and 37°C for 1 h and plated on LB agar plates containing 34 μg/ml chloramphenicol and incubated for 37°C overnight.

The next day, single colonies were picked to inoculate 5 ml LB cultures, which were miniprepped and confirmed by Sanger sequencing (Quintara Biosciences). Correct constructs were re-transformed into 10-beta chemically competent cells (NEB), plated on LB agar plates containing chloramphenicol, and incubated for 37°C overnight. The next day, single colonies were picked to inoculate 6 ml LB cultures, which were used to generate duplicate 1 ml glycerol stocks (25% glycerol, stored −80°C) and miniprepped. Sequences were again confirmed by Sanger sequencing (Quintara Biosciences). Sequences of all riboswitch variants can be found in Supplementary Data File 1 along with Addgene accession numbers for select variants.

In vivo bulk fluorescence reporter assay

Fluorescence assays were performed in *E. coli* BW25113 (Keio collection parent strain). Riboswitch expression plasmids tested in each experiment were transformed into chemically competent *E. coli* BW25113 cells, recovered in a benchtop shaker at 1000 rpm and 37°C for 1 h, plated on LB agar plates containing 34 mg/ml chloramphenicol, and incubated overnight at 37°C. The following day, plates with *E. coli* colonies were removed from 37°C and stored at room temperature for approximately 7 hours. For each construct, three colonies corresponding to three biological replicates were used to inoculate separate 300 μl cultures of LB media containing 34 mg/ml chloramphenicol in 2 ml 96-well culture blocks covered by breathable seals, which were incubated in a benchtop shaker at 1000 rpm and 37°C overnight. After overnight incubation for 16 hours, cultures from each biological replicate were used to inoculate a subculture. Each subculture was assembled by combining 4 μl of overnight culture with 194 μl freshly prepared M9 enriched media (1× M9 salts, 1 mM thiamine hydrochloride, 0.4% glycerol, 0.2% casamino acids, 2 mM $MgSO_4$, 0.1 mM $CaCl_2$, 34 mg/ml chloramphenicol) and 2 μl DMSO containing 100x desired final concentration of 5-aminoimidazole-4-carboxyamide-ribonucleoside (Z) (Millipore Sigma) in 2 ml 96-well culture blocks. Separately prepared stocks of M9 salts, glycerol, casamino acids, $MgSO_4$, and $CaCl_2$ were used for each experimental replicate (group of three biological replicates). After assembly, biological replicate subcultures were covered with breathable seals and incubated in a benchtop shaker at 37°C and 1000 rpm for 6 h unless otherwise indicated. Samples for fluorescence analysis were prepared after incubation by combining 50 μl of exponential phase cells with 50 μl 1× phosphate buffered saline (PBS) in flat-bottom optically clear plates. Fluorescence measurements (485 nm excitation, 528 nm emission) and OD_{600} were taken on a Biotek Synergy H1 plate reader with the gain set to 70. All *in vivo* reporter assays were performed with three experimental replicates, each performed with triplicate biological replicates for a total of nine data points ($n = 9$) per mutant.

Data analysis was performed by subtracting the average blank (50 μl M9 enriched media + 50 μl 1× PBS alone) OD_{600} and fluorescence measurements from the values collected for each sample-containing well. Corrected fluorescence values (arbitrary units) for each well were divided by corrected OD_{600} values for that same well, to normalize fluorescence values to the number of cells in each well. All statistical analysis (mean, standard deviation, t-tests with Bonferroni correction, curve-fitting) was performed on background corrected, normalized fluorescence values. EC_{50} values were determined by fitting dose response curves to the formula $Normalized\ fluorescence = a + b\frac{[Z]}{EC_{50}+[Z]}$ where [Z] denotes ligand concentration in the media, a scales the curve to the minimum response and b scales the curve to the maximum response. Fitting was performed using DataGraph 5.0.

Single round *in vitro* transcription functional assay

Linear templates for *in vitro* transcription (IVT) were generated from plasmids via PCR using primers ordered from Integrated DNA Technologies (IDT). Using New England Biosciences (NEB) Phusion® High-Fidelity PCR Kit, 2 ml PCRs were assembled with 1–10 ng/μl DNA template, 200 μM dNTPs (NEB), 1× Phusion® HF Buffer, 400 nM each of forward and reverse primers, and 5 μl Phusion® polymerase (2000 U/ml). PCR products were run on 1% agarose gels to confirm amplification of the desired length product, and PCR cleanup was performed with buffers from the QIAquick PCR Purification Kit (Qiagen) using EconoSpin® All-in-One mini spin columns (Epoch Life Science). IVT

linear template was eluted from spin columns using 50 μl UltraPure™ DNase/RNase-Free Distilled Water (Invitrogen) and quantified using a NanoDrop™ One Spectrophotometer (Thermo Scientific).

25 μl reactions were prepared containing 90 nM linear DNA template, 0.5 μl 50× Z in DMSO, transcription buffer (20 mM Tris–HCl, pH 8.0, 0.1 mM EDTA, 1 mM DTT, 5 mM $MgCl_2$ and 50 mM KCl), 0.1 mg/ml BSA (NEB), and 1.25 μl of *E. coli* RNAP holoenzyme (NEB). The reaction tube was incubated at 37ºC for 10 minutes to form open transcription complexes, and then started with NTPs (final concentration of 400 μM ATP, GTP, CTP, UTP) and rifampicin at 10 μg/ml. Transcription was allowed to proceed for 30 s at 37ºC and then stopped by the addition of 75 μl TRIzol™ Reagent (Invitrogen).

RNA extraction and purification was performed by adding 20 μl chloroform (Millipore Sigma) and spinning for 5 min at 4ºC. 70 μl of the aqueous phase was transferred to a new tube containing 50 μl isopropanol (Millipore Sigma) and 1 μl glycogen coprecipitant (Invitrogen). Samples were incubated at room temperature for 20 min, pelleted by spinning at 4ºC for 45 min, aspirated, and washed with 500 μl 70% ethanol. Dried pellets were resuspended in 1× TURBO™ DNase Reaction Buffer (Invitrogen) and 1 μl TURBO™ DNase and incubated at 37º for 1 h. Following digestion, RNA extraction and purification was performed using 150 μl TRIzol™ Reagent (Invitrogen) and 40 μl chloroform (Millipore Sigma). 140 μl of the aqueous phase was extracted and transferred to a new tube containing 100 μl isopropanol and 1 μl glycogen coprecipitant (Invitrogen). RNA was pelleted by spinning at 4ºC for 45 min, and aspirated and washed with 70% ethanol. Dried pellets were resuspended in 10 μl UltraPure™ DNase/RNase-Free Distilled Water (Invitrogen) and 10 μl 2X RNA Loading Dye (NEB), denatured at 95º for 5 min, and run on an 8% denaturing gel made using reagents from the SequaGel® UreaGel™ System (National Diagnostics). Gels were stained with SYBR™ Gold Nucleic Acid Gel Stain (Invitrogen) and imaged on a ChemiDoc™ Touch Imaging System (BioRad). Fraction read through was calculated by defining terminated and anti-terminated bands using Image Lab 6.1 (BioRad) and recording the band percent for the anti-terminated band.

RESULTS

Developing an *in vivo* reporter assay to characterize riboswitch function

We began by developing an expression construct that would allow us to characterize riboswitch function *in vivo* using cellular gene expression assays. The expression construct consisted of the well-characterized *Cbe pfl* ZTP riboswitch sequence placed downstream of a J23119 constitutive *E. coli* σ^{70} promoter as previously described (15), followed by a strong ribosome binding site and a superfolder GFP (sfGFP) coding sequence (Figure 1B, Supplementary Data File 1). This construct was then placed within a p15A plasmid backbone with chloramphenicol resistance. Following an experimental design by Kim and colleagues (27), who used direct treatment of *E. coli* with Z to induce a β-galactosidase expression cassette, we transformed this plasmid into *E. coli* strain BW25113, picked colonies, grew overnight cultures, and sub-cultured with and without Z added directly to the media (Materials and Methods, Figure 1B). Endpoint bulk fluorescence and optical density (OD_{600}) measurements were made after 6 h of subculture in the presence or absence of different amounts of Z. We selected 6 h as our endpoint measurement because this time point showed robust fold-changes between the no ligand and saturating ligand (1 mM) conditions (Supplementary Figure S1A). Under these conditions, we found that the addition of Z did not affect growth rate (Supplementary Figure S1B), and that this riboswitch expression construct responded comparably to Z and ZMP supplied to the media (Supplementary Figure S1C). Using this *in vivo* reporter assay, we characterized riboswitch dose-response by adding a range of Z concentrations to the media (Figure 1C), which showed similar dose-response characteristics to those observed using *in vitro* transcription (15).

Using the *in vivo* assay, we next characterized a riboswitch mutant broken in the OFF functional state. Following previous mutational analysis of the PK region which rendered the riboswitch unresponsive to induction by ZMP (15), we selected A26Δ as the OFF control. Characterization of this mutant with several Z concentrations showed the expected effects (Figure 1D). All subsequent mutational analysis was also carried out in the A26Δ background as a negative control, which allowed us to distinguish between mutations that truly affect the anti-termination decision and mutants that affect baseline termination efficiency alone. Taken together, these results establish an *in vivo* assay for functional characterization of *Cbe pfl* riboswitch mutants.

Cbe pfl riboswitch EP sequence and structure features tune dynamic range

A key goal of this study was to interrogate how specific features of the *Cbe pfl* ZTP EP determine riboswitch function *in vivo*. The key conformational change enabling switching behavior in the cotranscriptional folding pathway of the ZTP riboswitch is strand displacement of the AD P3 helix by the 3' invader (Figure 2A). This step is necessary in order to disrupt the AD and form the terminator in the OFF state, but must be blocked in order to allow transcription to proceed in the ON state. How this strand displacement process is governed by EP sequence and structure remains poorly understood. We therefore sought to interrogate this critical conformational change by identifying nucleotides in the terminator invader that are important for regulatory function. Previous smFRET experiments with the *Fusobacterium ulcerans* ZTP riboswitch showed that mutating the first three nucleotides of the invader to A severely delayed formation of the terminator hairpin (13), inspiring us to interrogate the invader with fine-grained functional mutagenesis.

We disrupted the formation of each base pair of the terminator by mutating each nucleotide of the invader in two ways: either with a mismatch mutation (Figure 2B), or by deleting each nucleotide (Supplementary Figure S2A). Gene expression analysis of these variants in the presence of varying amounts of Z showed that the base pair interactions closest to the strand displacement nucleation site (top of the terminator hairpin) have the biggest effect on

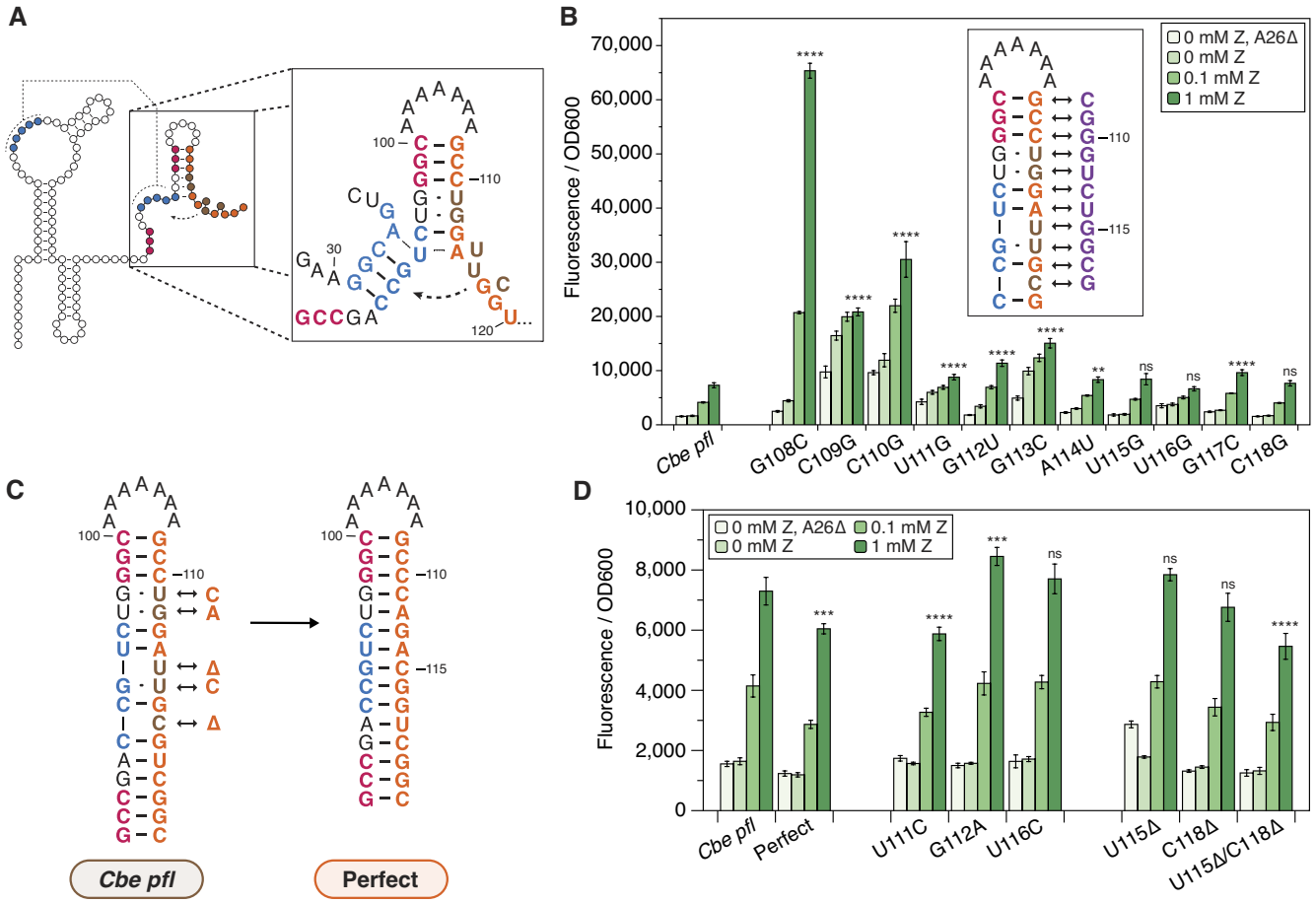

Figure 2. Noncomplementary elements in the expression platform tune the ON state of the *Cbe pfl* ZTP riboswitch. (**A**) Diagram of the strand displacement process during terminator formation. The invader (orange) nucleates the terminator hairpin by base pairing with the 3' nucleotides of the P3 stem (red), enabling branch migration through the pseudoknot (PK, blue). Noncomplementary elements (mismatches, bulges) of the invader are shown in brown. (**B**) Mismatch scan of the invader showing position-dependent effects of mismatch mutations on fluorescence, mostly affecting expression when Z is present. Asterisks indicate the significance threshold α for pairwise t-tests between the observed fluorescence from a particular mutation vs. that from the wildtype construct at the 1mM ZTP condition. (**C**) Diagram highlighting the noncomplementary elements of the natural invader (brown), and the mutations performed to generate a perfectly complementary invader. (**D**) Mutational scan to eliminate noncomplementary elements individually, or all at once (perfect). Noncomplementary elements are grouped into wobble pairs (center) or bulges (right). Asterisks indicate the significance threshold α for pairwise t-tests between the observed fluorescence from a particular mutation vs. that from the wildtype construct at the 1 mM Z condition. Bars in (B) and (D) represent averages from three experimental replicates, each performed with triplicate biological replicates for a total of nine data points ($n = 9$), with error bars representing standard deviation. *t*-test significance thresholds are for pairwise (two-tail, heteroscedastic) tests with values prior to Bonferroni correction of: *α = 0.05, **α = 0.01, ***α = 0.001, ****α = 0.0001, ns = not significant.

riboswitch dynamic range, consistent with the observations of Hua *et al.* (13). Specifically, we found that mutating the terminator nucleating base pair (C100:G108) to either a mismatch (G108C) or a deletion (G108Δ) resulted in a significantly higher dynamic range than the wildtype riboswitch (Figure 2B, Supplementary Figure S2A), suggesting that the formation of the wildtype GC pair in this position has a dampening effect that limits the natural ON state. Sequence changes further down the terminator hairpin have progressively smaller effects on dynamic range (Figure 2B, Supplementary Figure S2A). Surprisingly, the C118G mismatch mutation, which should disrupt a previously described RNAP pause site, did not result in any significant change in ON-state gene expression (Figure 2B). Other C118 mutants did not show large differences in sensitivity or dynamic range compared to wild type (Supplementary Figure S2B-D), indicating that this pause site does not play an important role in riboswitch function. Taken together, these results align with previous observations from DNA nanotechnology that mismatch mutations closer to the strand displacement initiation site have larger effects on the strand displacement rate than more distal mismatch mutations (20–22).

Based on these results, we reasoned that noncomplementary base pairing features present in the natural sequence of the invader could pose kinetic barriers to strand displacement, disfavoring the formation of the terminator hairpin. Specifically, the wildtype *Cbe pfl* invader features five non-complementary elements relative to the sequence that it invades: three wobble pairs and two single-nucleotide bulges (Figures 1A, 2C; brown). To test if these wobble pairs and bulges moderate the kinetics of strand displacement to achieve higher baseline expression and/or higher ON state, we 'corrected' the invader to perfectly

complement the substrate strand contained in the AD (Figure 2C). We also characterized the effect of making each of these corrective mutations individually. We observed that the perfectly complementary invader resulted in significantly lower ON state than wildtype *Cbe pfl* (Figure 2D), and of the five individual corrective mutations, the correction of the wobble pair most proximal to the strand displacement nucleation site (U111C), decreased the ON state the most (Figure 2D). While deleting either the U115 or C118 bulges individually did not significantly affect the ON state, deleting both bulges simultaneously resulted in a substantial decrease in ON state compared to the wild type (Figure 2D). Interestingly, the G112A corrective mutation increased ON-state fluorescence compared to the wild type, suggesting that the natural U96:G112 wobble pair facilitates more efficient strand displacement through P3 than a Watson–Crick pair at this position. In total, these results show that the *Cbe pfl* ZTP riboswitch EP contains sequence features that tune dynamic range by moderating the kinetics of strand displacement.

Clostridium genus ZTP riboswitches contain EP elements that tune dynamic range

Having established that the *Cbe pfl* ZTP riboswitch uses noncomplementary elements to tune ON-state gene expression by moderating the kinetics of strand displacement, we hypothesized that other *Clostridium* genus ZTP riboswitches may employ similar mechanisms to match riboswitch function to cellular needs. To investigate this hypothesis, we first performed a bioinformatic analysis of EP sequence variation within ZTP riboswitches. All *Clostridium* genus ZTP riboswitch sequences from the RFam database (73 sequences) were aligned, and first narrowed to include only those sequences that contain a putative terminator poly-U tract of at least 5 Us and an identical P3 sequence to the *Cbe pfl* riboswitch, which resulted in 18 curated sequences. We next identified those sequences which feature a loop + invader architecture similar to the *Cbe pfl* riboswitch based on secondary structure prediction of the terminator hairpin using NUPACK (15 sequences) (31).

From this set, we selected a subset of expression platform variants that (i) possessed a unique invader and (ii) which natively regulate a gene also regulated by at least one other riboswitch in the subset, for a final subset of 12 *Clostridium* genus ZTP riboswitches, including a second ZTP riboswitch from *C. beijerinckii*. For each subset member, we created a chimeric riboswitch consisting of the *Cbe pfl* AD (including the P3 sequence shared among all sequences) and the invader of the variant of interest (Figure 3A). Cellular gene expression assays of the eight functional chimeras using a range of Z concentrations showed that variations in the invader sequence (Supplementary Data Table S1) led to differences in functional properties of the chimeric riboswitches (Figure 3A).

Consistent with our previous observations, invaders with kinetic barriers to strand displacement near the top of the terminator hairpin showed higher ON-state fluorescence than the perfectly complementary invader (Figure 3A). To validate these results, we determined the functional effect of all non-complementary sequence elements from these riboswitches in the perfect invader background (Figure 3B). These results allowed us to demarcate regions of the invader responsible for tuning the ON state and the leak level, as well as a variable region relatively insensitive to mutation (Figure 3A, B). The most common non-complementary elements observed in this subset of EPs were wobble pairs and mismatches. Consistent with the results of Figure 2D, we observed that the U:G wobble pair formed by the A112G mutation resulted in lower ON-state fluorescence than a U:A Watson–Crick pair.

Interestingly, we observed that invaders from riboswitches that regulate the same genes result in functionally similar chimeric riboswitches *in vivo* (Figure 3A). For example, *purH*-regulating riboswitches all show elevated ON-state fluorescence relative to the perfectly complementary invader, which can be attributed to the common C110U wobble pair mutation. All of these chimeras also show elevated baseline expression compared to the perfectly complementary invader (Figure 3A). This increase in leak is attributable the presence of a G:G mismatch near the base of the terminator hairpin (Figure 3B), consistent with known structure rules dictating intrinsic terminator strength (32,33). In the case of ZTP riboswitches that regulate *pflA*, the resulting chimeric riboswitches were nearly functionally identical, despite deviations in the sequence of the invaders (Figure 3A). Taken together, these findings suggest that natural ZTP riboswitches could have evolved to exploit strand displacement kinetics to tune expression in different regulatory contexts.

Kinetic barriers to strand displacement tune ON-state fluorescence

Taking inspiration from the natural strategy employed at least by *Clostridium* ZTP riboswitches to tune ON-state gene expression with noncomplementary features in the invader, we next sought to perform fine-grained analysis of how different mutation types at different positions in the invader alter dynamic range (Figure 4A). We chose to perform this mutagenesis analysis in the context of the perfectly complementary invader (Figure 2C) so we could measure the effect of each mutation in isolation.

We first tested the addition of single-nucleotide bulges at different possible positions within the invader in order to slow strand displacement and thus disfavor terminator formation. As expected, we found that these mutations resulted in an increase in ON-state gene expression in a position-dependent manner (Figure 4B). Interestingly, the A-bulge at position 1 affected EC50, indicating that early events in the strand displacement pathway could affect sensitivity; though this effect was not observed for any other position (Figure 4C).

To extend this analysis, we performed similar mutational scans by inserting di- and tri-nucleotide bulges, which we expected to pose larger barriers to strand displacement than a single-nucleotide bulge, as well as mismatches, deletions, and wobble pairs. All of these mutational scans resulted in similar position-dependent increases in ON-state fluorescence relative to the perfectly complementary invader scaffold, though they appeared to have a different magnitude of effect depending on the type of mutation introduced

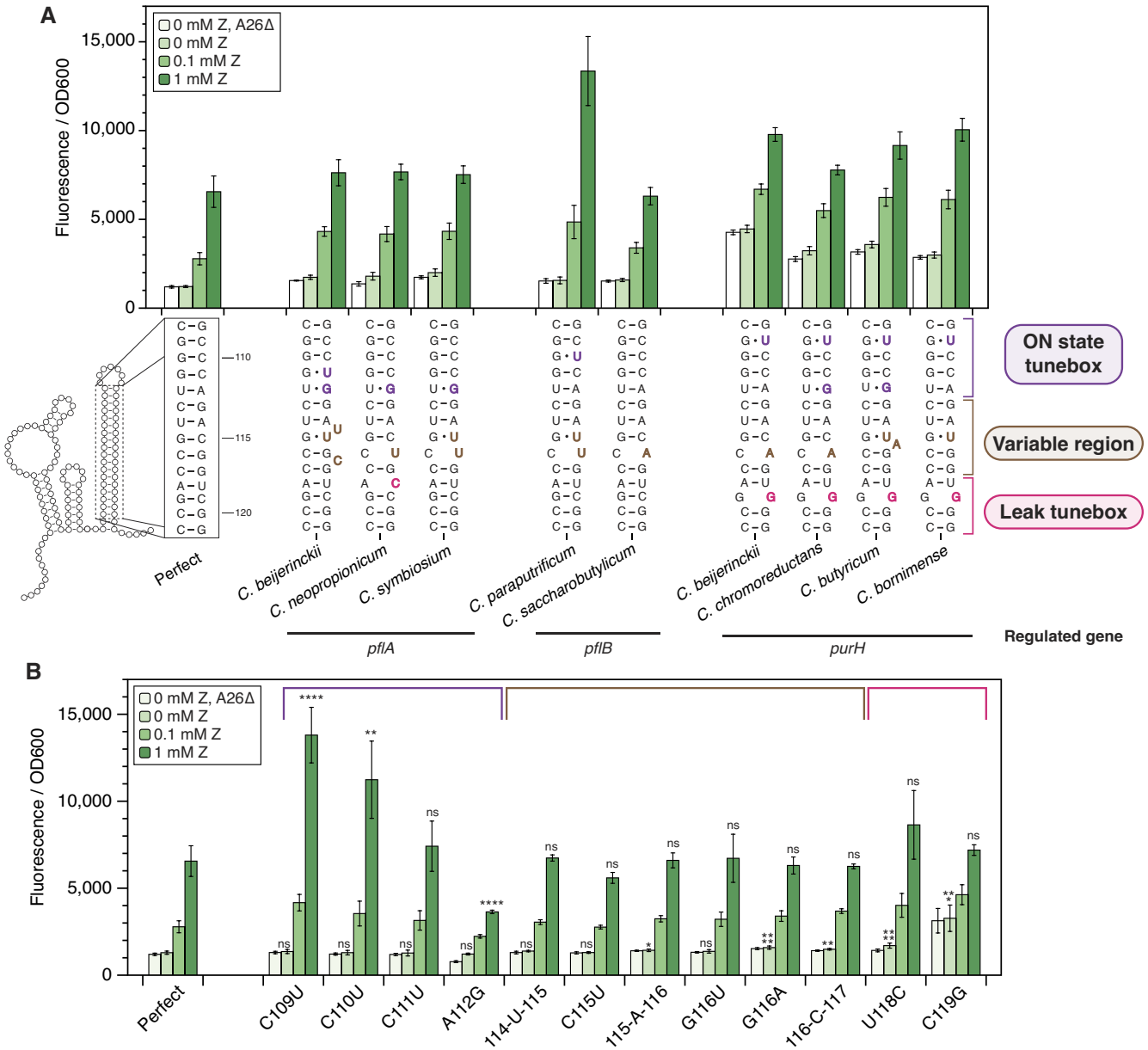

Figure 3. Other *Clostridium* ZTP riboswitch expression platforms tune ON and OFF states with kinetic barriers to strand displacement. (**A**) Gene expression characterization of chimeric riboswitches, constructed by fusing the *Cbe pfl* riboswitch aptamer sequence (containing the 5' portion of the expression platform) with the 3' invader of the expression platform of different *Clostridium* species. Putative terminator hairpin secondary structures (noncomplementary elements in bold) are below observed gene expression under varying ZTP concentration conditions. Sequences are grouped by the gene they regulate in their native genomic context (Supplementary Table S1). Bolded sequence elements are colored according to their position within the annotated regions of the invader. (**B**) Functional characterization of all individual noncomplementary elements from natural *Clostridium* ZTP riboswitch expression platforms characterized in (A) in the context of the perfectly complementary terminator (Figure 2C). Insertion mutations are bracketed by position numbers. Based on the magnitude of functional effects, these mutations are divided into three functional domains: the ON-state tunebox (purple), the variable region (brown), and the leak tunebox (fuchsia). Bars represent averages from three experimental replicates, each performed with triplicate biological replicates for a total of nine data points ($n = 9$), with error bars representing standard deviation. Asterisks indicate significance threshold α for pairwise t-tests (two tailed, heteroscedastic) between the observed fluorescence from a particular mutation versus that from the *pfl* construct with perfect expression platform pairing at the Z condition indicated on the bar prior to Bonferroni correction: *$\alpha = 0.05$, **$\alpha = 0.01$, ***$\alpha = 0.001$, ****$\alpha = 0.0001$.

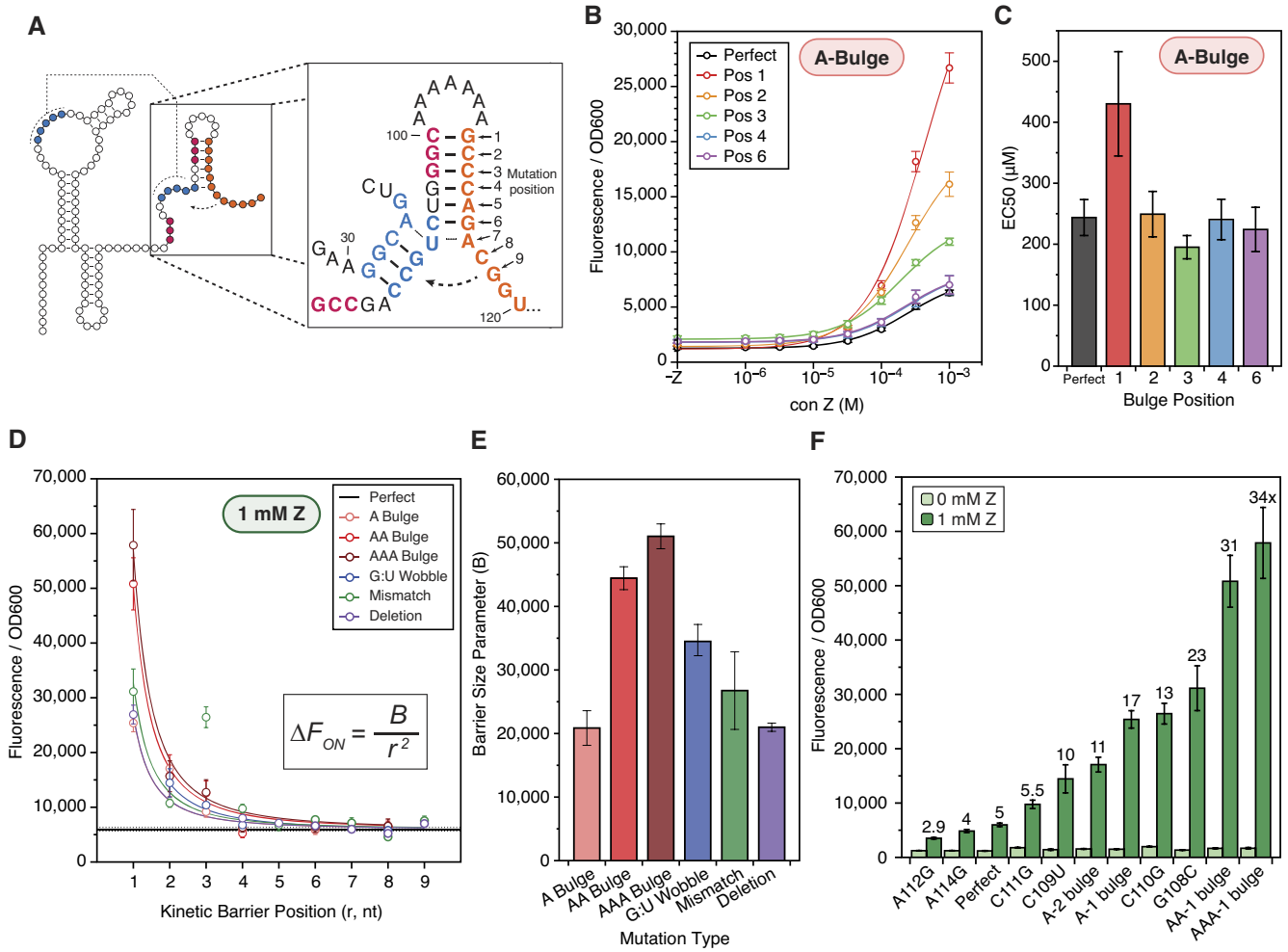

Figure 4. Kinetic barriers to strand displacement enable fine-grained control of riboswitch dynamic range. (**A**) Diagram of the strand displacement process during terminator formation in the context of the perfectly paired terminator (Figure 2C). The invader (orange) nucleates the terminator hairpin by base pairing with the 3' nucleotides of the P3 stem (red), enabling branch migration through the PK (blue). Positions mutated in subsequent panels are indicated by a numerical index. Bulge mutations were inserted immediately after the nucleotide identified by the position index (e.g. A bulge at position 3 denotes an insertion between C110 and C111). (**B**) Dose response curves for various A-bulge mutants. (**C**) EC50s extracted from sigmoidal fits of the data in panel B showing the effect of A-bulge mutations on riboswitch sensitivity. Error bars indicate standard error of the fit parameter. (**D**) The measured ON state of gene expression assays with 1 mM Z from scans with different mutations including bulge insertions (A, AA, AAA), wobble pairs, mismatch pairs and deletions, each at the different indicated positions within the terminator. The perfectly complementary expression platform fluorescence (1 mM Z) is shown as a dashed line. Full data in Supplementary Figure S3 A-E. Data are fit to the inset equation, where ΔF is the increase in ON-state fluorescence for each mutant compared to the perfect terminator ON-state fluorescence (1 mM Z), and the parameter B characterizes the kinetic 'barrier size for strand invasion. (**E**) The kinetic barrier size parameter, B, extracted from the fits plotted in (D), showing the relative effects of different mutation types on ON-state fluorescence. Error bars indicate standard error of the fit parameter. (**F**) Gene expression characterization of select kinetic barrier mutants showing widely varying dynamic range. Fold-change between 1 mM and 0 mM Z conditions is indicated by a label above each mutant. Error bars indicate standard deviation. Points in (B) and (D) and bars in (F) represent averages from three experimental replicates, each performed with triplicate biological replicates for a total of nine data points ($n = 9$), with error bars representing standard deviation.

(Figure 4D–F, Supplementary Figure S3A–E). Consistent with previous results, we observed that mutations changing U:A Watson–Crick pairs to U:G wobble pairs (A112G and A114G) resulted in position-dependent *decreases* in ON-state fluorescence relative to the perfectly complementary invader (Figure 4F, Supplementary Figure S3C).

To determine the extent to which increases in ON-state fluorescence could be attributed to the change in thermodynamic stability of the terminator hairpins caused by the mutations, we performed conformational free energy calculations for all kinetic barrier mutants using NUPACK (Supplementary Figure S4). For all but the G:U wobble mutants we observe either a flat or opposite position-dependent trend compared to the observed dynamic range (Supplementary Figure S4B), indicating that terminator free energy does not explain the observed patterns of positional dependence on dynamic range.

To better understand the difference in magnitude between different types of mutations at a phenomenological level, we fit the observed position-dependent ON state values to the power law curve $\Delta F_{ON} = \frac{B}{r^2}$, where ΔF_{ON} is the increase in ON-state fluorescence for each mutant compared to the perfect terminator ON-state fluorescence, r is the position of the mutation in nucleotides from the

strand displacement nucleation site (terminator loop), and *B* describes the magnitude of the decay trend (Figure 4D). Plotting the fitted *B* values for each type of mutation showed that the trend was single nt bulge = deletion < mismatch ≤ G:U wobble < double nt bulge < triple nt bulge (Figure 4E). This aligns with the interpretation that the larger the barrier to strand displacement that each mutation produces, the larger the phenomenological *B* value.

Overall, these results show that introducing kinetic barriers to strand displacement by mutating the invader enables fine-tuning of riboswitch dynamic range *in vivo* from 2.4- to 34-fold (Figure 4F), and placing larger kinetic barrier mutations closer to the initiation of strand displacement causes the largest effect.

Kinetic strand displacement barriers can be used to tune the dynamic range of a synthetically flipped-logic ZTP riboswitch

As a final demonstration of the importance of strand displacement barriers for tuning riboswitch decision-making, we sought to apply our understanding from the studies above to tune the functional performance of a version of the *Cbe pfl* ZTP riboswitch that features an additional competing strand displacement process. In a recent study of the *yxjA* purine transcriptional OFF-riboswitch, it was discovered that this riboswitch flips the typical transcriptional ON regulatory logic through the presence of an additional intermediate structure (11). Inspired by this observation, we inverted the regulatory logic of the *Cbe pfl* ZTP riboswitch by inserting an 8-nt 'flipping domain' after the intrinsic terminator hairpin (Figure 5A). In the absence of ligand, this flipping domain is designed to act as a spacer between the wildtype intrinsic terminator hairpin and the poly-U tract, thus ablating termination and producing an ON regulatory state. In the presence of ligand however, the flipping domain was designed to base pair with the remaining portion of the wildtype invader left over from failed strand displacement of the AD, creating a new synthetic intrinsic terminator hairpin adjacent to the poly-U tract and resulting in an OFF regulatory state. As expected, this synthetic OFF-riboswitch functions at the level of transcription, though it exhibits poorer dynamic range than the wildtype ON-switch *in vitro* (Figure 5B, Supplementary Figure S5-8) and *in vivo* (Figure 5C).

We reasoned that the observed high leak level in the ligand-induced OFF state was the result of an inherent bias toward the formation of the wildtype terminator hairpin, which in this flipped context would result in a bias towards the ON state. Based on our understanding of strand displacement barriers, we hypothesized that inserting kinetic barriers into the invader would reduce this bias and thereby improve dynamic range. In this context, the G108Δ deletion, which increases the ON state of the *Cbe pfl* riboswitch >3× (Supplementary Figure S2A), significantly decreases the leak of the flipped-logic OFF-switch (Figure 5C). Larger kinetic barriers, including a di- or tri-nucleotide bulge in between G108 and C109, result in greater decreases in OFF state leak (Figure 5C), indicating that kinetic barrier size is correlated with the resulting dynamic range.

These results demonstrate the ability to flip the logic of transcriptional ON-riboswitches into OFF-riboswitches using synthetic sequences, and further show how the application of simple mutations to slow strand displacement at key points of the riboswitch mechanism can be used to enhance the dynamic range of synthetic transcriptional OFF riboswitches as well.

DISCUSSION

There is a growing appreciation for the apparent ubiquity of DNA and RNA mechanisms that feature strand displacement-mediated conformational switching (34). Processes at the heart of genome maintenance and gene expression such as homologous recombination, spliceosomal activation and large ribosomal subunit maturation are thought to be facilitated by strand displacement-mediated rearrangements (17,35,36). However, there are still large gaps in our knowledge of how biology tunes these processes *in vivo* (17,34). Recent work has shown that several classes of transcriptional riboswitches feature an internal strand displacement process at the core of their folding pathways, which enables EPs to both sense AD-ligand binding state and commit to a gene-regulatory decision based on the outcome of this attempted conformational switch. In this work, we observed that the *Cbe pfl* ZTP riboswitch balances this cotranscriptional conformational switching with a combination of sequence and structure features that both favor and disfavor efficient strand displacement.

On the one hand, noncomplementary sequence elements in the EP invader act to moderate strand displacement kinetics and increase ON-state gene expression. On the other hand, the wildtype EP forms several strong nucleating base pairs at the initiation of strand displacement, the disruption of which 'unlocks' drastic increases in dynamic range. Increases in ON-state gene expression compared to a perfectly complementary invader rely on two factors: the type of kinetic barrier mutation introduced, and the proximity of that kinetic barrier to the strand displacement nucleation site. These trends are consistent with previous work showing that the effect of mismatch mutations on the rate of strand displacement is strongly dependent upon the position of the mismatch relative to the strand displacement nucleation site (21,22). A recent study of the *Fusobacterium ulcerans* ZTP riboswitch showed that mutations to the EP invader severely slowed the rate of terminator formation *in vitro* (13), supporting our conclusion that riboswitch conformational switching can be tuned by modulating strand displacement kinetics. Further, an analysis of the effects of the kinetic barrier mutations on predicted free energy of the terminator hairpin showed that equilibrium hybridization strength of the terminator cannot explain differences in riboswitch function (Supplementary Figure S4B). Interestingly, while wobble mutations that convert G:C pairs to G:U pairs achieve similar phenotypes as other kinetic barrier mutations, in different contexts we observe that U:G wobble pairs appear to favor strand displacement relative to U:A Watson–Crick pairs (Figure 4F, Supplementary Figure S3C). To our knowledge, this is the first observation of non-Watson-Crick base pairs enhancing strand displace-

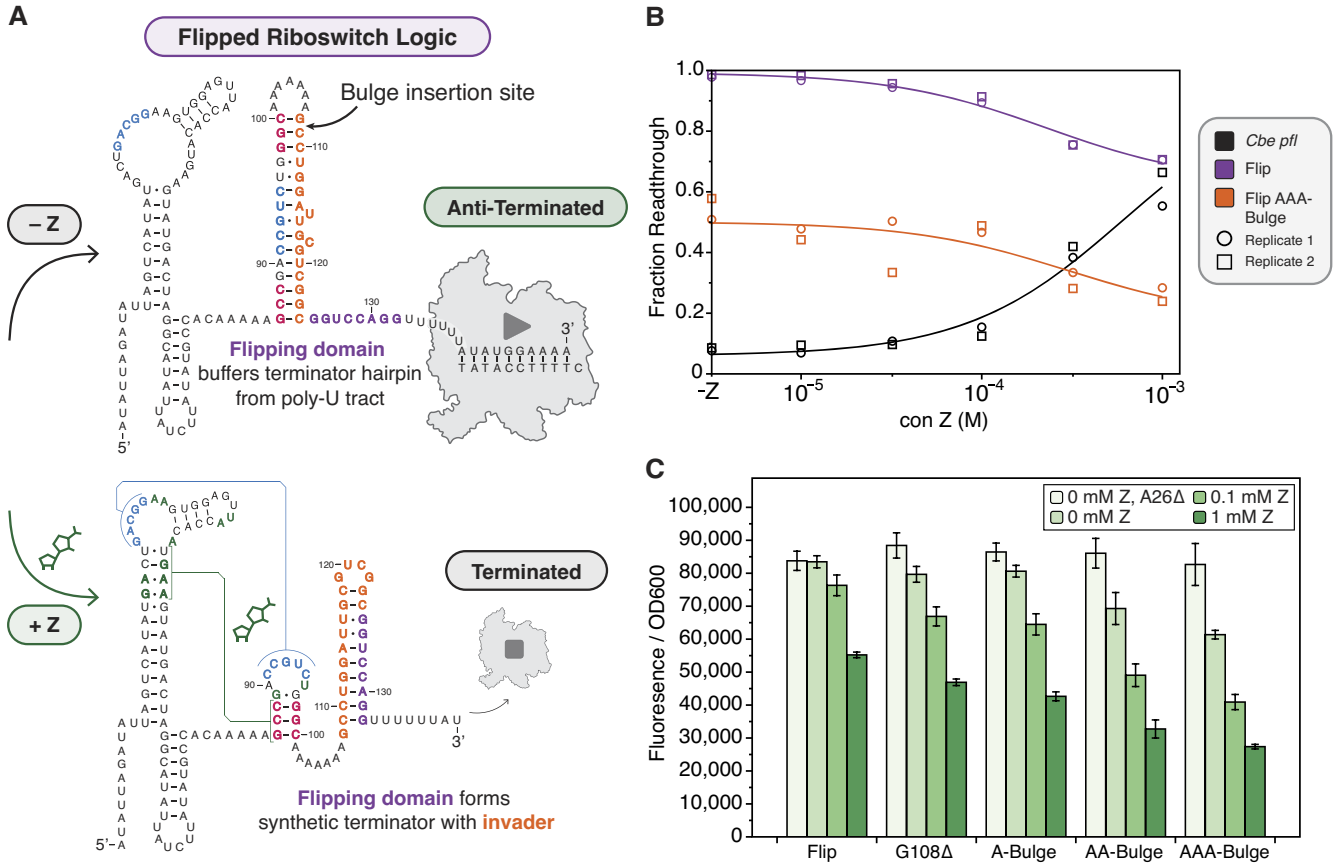

Figure 5. Kinetic barriers to strand displacement tune the dynamic range of a synthetic 'flipped-logic' ZTP riboswitch. (**A**) Schematic detailing the approach for inverting the logic of the *Cbe pfl* ZTP riboswitch from an ON-switch to an OFF-switch. In the absence of ligand, an eight nucleotide insertion, named the 'flipping domain' (purple), is designed to ablate intrinsic termination by increasing the spacer between the ZTP riboswitch terminator hairpin and its poly-U tract. In the presence of ligand, however, the flipping domain is designed to form a synthetic terminator with the portion of the expression platform that results from unsuccessful strand displacement of the aptamer. Areas in the expression platform where sequence deletions or bulge insertions can tune dynamic range are indicated. (**B**) Single round *in vitro* transcription results ($n = 2$) validating the functionality of the 'Flip' design and the functional improvement imparted by a tri-nucleotide bulge between G108 and C109. Source gels are available in Supplementary Figures S5–S8. (**C**) *In vivo* validation of the 'Flip' design showing successive improvements in dynamic range when successively larger kinetic barriers to strand displacement of the aptamer are added to the expression platform at the position indicated in (A). Bars in (C) represent averages from three experimental replicates, each performed with triplicate biological replicates for a total of nine data points ($n = 9$), with error bars representing standard deviation.

ment efficiency, and it is not clear whether this is a general phenomenon or one peculiar to this system.

A quantitative look at which types of sequence variations led to the largest changes in riboswitch function shows that there may be limits to how much tuning strand displacement can alter riboswitch function. While most kinetic barrier mutations had minimal impact on riboswitch leak, the kinetic barriers with the largest B values in this study, di- and tri-nucleotide bulges, produced large increases in uninduced gene expression when placed at positions proximal to the strand displacement nucleation site (Supplementary Figure S3B). Interestingly, these increases in leak are not observed in the PK-incompetent A26Δ background (Supplementary Figure S3A), suggesting that sufficiently large kinetic barriers to EP strand displacement can disfavor formation of the terminator hairpin enough to allow a subpopulation of apo-ADs to withstand displacement long enough to yield an anti-termination decision. Taken together, these results point to inherent limits in the switching efficiency achievable by tuning strand displacement alone.

This work also sheds light on two important general questions in riboswitch biology: (i) Why are EPs so poorly conserved relative to ADs and (ii) How can bacteria regulate multiple genes at different baseline levels with the same riboswitch class? In this work, we observed that EPs from different *Clostridium* species with multiple different point mutations can achieve nearly identical functional profiles (the same baseline and ON-state gene expression). A more detailed analysis shows that the ZTP riboswitch EP contains distinct regulatory regions that affect different aspects of gene expression. Overall, this supports the view that poor EP conservation arises partly because there are many possible EP sequences that can meet evolutionary selection pressures on function. Importantly, the mechanistic basis of how sequence variation in the EP leads to leak and ON-state tuning requires only the *disruption of* base pairing to provide a kinetic barrier to strand displacement, in contrast to mutational covariation needed to preserve RNA structures in ADs during riboswitch evolution. Thus EP sequence variation may offer a simpler evolutionary route to tuning

riboswitch function than AD sequence variation. We hope these observations can be used to inform new bioinformatic analyses that can further uncover patterns in EP sequence evolution. A limitation of the approaches used in this study is that functional assays were performed in the heterologous model organism *E. coli*, limiting our ability to assess possible functional effects of sequence variants in the native organism.

Our work in creating a synthetically flipped OFF ZTP riboswitch also synergizes with recent studies of natural transcriptional OFF-riboswitches. Recently we showed that the *yxjA* purine OFF-switch contains an additional 'central helix' intermediate structure, formed cotranscriptionally in between the AD and EP, that serves to introduce an additional competing strand displacement process that inverts the regulatory logic from the typical ON adenine/guanine riboswitch mechanism (11). Work from Schwalbe and colleagues also recently highlighted a contrasting pair of cyclic-di-nucleotide-sensing riboswitches with opposite transcriptional logic, with the Cd1 OFF-switch EP featuring an additional competing structure relative to the simpler pilM ON-switch, resulting in inverted regulatory logic (37). In this context, our introduction of a synthetic 'flipping domain' converts the ZTP terminator hairpin into a central-helix-like element, and introduces an additional competing strand displacement process that flips the regulatory logic. This points to a potentially generalizable mechanism of converting transcriptional ON-switches into OFF-switches through the insertion of additional sequences, and vice versa, which could have implications for riboswitch evolution.

Finally, we believe this work has implications for biotechnological applications of riboswitches, and adds to the list of examples of tools that use the EP as a programmable scaffold to modulate riboswitch dynamic range (38). As ADs are extremely sensitive to mutation, and among the most highly conserved sequences known (39), engineering EPs appears to be a more fruitful approach of optimizing natural and synthetic riboswitches for diverse applications in diagnostics, gene-regulatory circuits, or reporters (40–42).

DATA AVAILABILITY

All data in this article are available in the online supplementary material.

SUPPLEMENTARY DATA

Supplementary Data are available at NAR Online.

ACKNOWLEDGEMENTS

We wish to acknowledge the helpful insight of all members of the Lucks lab, especially Dr Katherine Berman and Dr Luyi Cheng for discussions about flipping riboswitch logic, Laura Hertz and Reese Richardson for advice in bioinformatic analysis, and Edric Choi for critical review of figures. We also wish to thank Dr Narasimhan Sudarsan for helpful advice about selecting strains for *in vivo* riboswitch assays, and Dr Petr Šulc for helpful discussions about RNA strand displacement.

FUNDING

National Institutes of Health Research [R01GM130901]; National Institutes of Health Training Grant [T32GM008 382 to D.Z.B., in part] through the Northwestern University Molecular Biophysics Training Program. Funding for open access charge: NIH.
Conflict of interest statement. None declared.

REFERENCES

1. Mccown,P.J., Corbino,K.A., Stav,S., Sherlock,M.E. and Breaker,R.R. (2017) Riboswitch diversity and distribution. *RNA*, **23**, 995–1011.
2. Batey,R.T., Gilbert,S.D. and Montange,R.K. (2004) Structure of a natural guanine-responsive riboswitch complexed with the metabolite hypoxanthine. *Nature*, **432**, 411–415.
3. Ren,A., Rajashankar,K.R. and Patel,D.J. (2012) Fluoride ion encapsulation by Mg^{2+} ions and phosphates in a fluoride riboswitch. *Nature*, **486**, 85–89.
4. Ren,A., Rajashankar,K.R. and Patel,D.J. (2015) Global RNA fold and molecular recognition for a pfl riboswitch bound to ZMP, a master regulator of one-carbon metabolism. *Structure*, **23**, 1375–1381.
5. Martín,A.L., Mounir,M. and Meyer,I.M. (2020) CoBold: a method for identifying different functional classes of transient RNA structure features that can impact RNA structure formation in vivo. *Nucleic Acids Res.*, **49**, e19.
6. Rivas,E. (2020) RNA structure prediction using positive and negative evolutionary information. *PLoS Comput. Biol.*, **16**, e1008387.
7. Breaker,R.R. (2022) The biochemical landscape of riboswitch ligands. *Biochemistry*, **61**, 137–149 .
8. Scull,C.E., Dandpat,S.S., Romero,R.A. and Walter,N.G. (2021) Transcriptional riboswitches integrate timescales for bacterial gene expression control. *Front. Mol. Biosci.*, **7**, 607158.
9. Wickiser,J.K., Winkler,W.C., Breaker,R.R. and Crothers,D.M. (2005) The speed of RNA transcription and metabolite binding kinetics operate an FMN riboswitch. *Mol. Cell*, **18**, 49–60.
10. Chauvier,A., Ajmera,P., Yadav,R. and Walter,N.G. (2021) Dynamic competition between a ligand and transcription factor NusA governs riboswitch-mediated transcription regulation. *Proc. Natl. Acad. Sci. U.S.A.*, **118**, e2109026118.
11. Cheng,L., White,E.N., Brandt,N.L., Yu,A.M., Chen,A.A. and Lucks,J.B. (2022) Cotranscriptional RNA strand exchange underlies the gene regulation mechanism in a purine-sensing transcriptional riboswitch. *Nucleic Acids Res.*, **50**, 12001–12018.
12. Freida,K.L. and Block,S.M. (2012) Direct observation of cotranscriptional folding in an adenine riboswitch. *Science*, **338**, 397–400.
13. Hua,B., Jones,C.P., Mitra,J., Murray,P.J., Rosenthal,R., Ferré-D'Amaré,A.R. and Ha,T. (2020) Real-time monitoring of single ZTP riboswitches reveals a complex and kinetically controlled decision landscape. *Nat. Commun.*, **11**, 4531.
14. Steinert,H., Sochor,F., Wacker,A., Buck,J., Helmling,C., Hiller,F., Keyhani,S., Noeske,J., Grimm,S., Rudolph,M.M. *et al.* (2017) Pausing guides RNA folding to populate transiently stable RNA structures for riboswitch-based transcription regulation. *eLife*, **6**, e21297.
15. Strobel,E.J., Cheng,L., Berman,K.E., Carlson,P.D. and Lucks,J.B. (2019) A ligand-gated strand displacement mechanism for ZTP riboswitch transcription control. *Nat. Chem. Biol.*, **15**, 1067–1076.
16. Watters,K.E., Strobel,E.J., Yu,A.M., Lis,J.T. and Lucks,J.B. (2016) Cotranscriptional folding of a riboswitch at nucleotide resolution. *Nat. Struct. Mol. Biol.*, **23**, 1124–1131.
17. Hong,F. and Šulc,P. (2019) An emergent understanding of strand displacement in RNA biology. *J. Struct. Biol.*, **207**, 241–249.
18. LeCuyer,K.A. and Crothers,D.M. (1994) Kinetics of an RNA conformational switch. *Proc. Natl. Acad. Sci. U.S.A.*, **91**, 3373–3377.
19. Haley,N.E.C., Ouldridge,T.E., Mullor Ruiz,I., Geraldini,A., Louis,A.A., Bath,J. and Turberfield,A.J. (2020) Design of hidden thermodynamic driving for non-equilibrium systems via mismatch elimination during DNA strand displacement. *Nat. Commun.*, **11**, 2562.

20. Irmisch,P., Ouldridge,T.E. and Seidel,R. (2020) Modeling DNA-strand displacement reactions in the presence of base-pair mismatches. *J. Am. Chem. Soc.*, **142**, 11451–11463.
21. Liu,H., Hong,F., Smith,F., Goertz,J., Ouldridge,T., Stevens,M.M., Yan,H. and Šulc,P. (2021) Kinetics of RNA and RNA:DNA hybrid strand displacement. *ACS Synth. Biol.*, **10**, 3066–3073 .
22. Machinek,R.R.F., Ouldridge,T.E., Haley,N.E.C., Bath,J. and Turberfield,A.J. (2014) Programmable energy landscapes for kinetic control of DNA strand displacement. *Nature Commun.*, **5**, 5324.
23. Olson,X., Kotani,S., Padilla,J.E., Hallstrom,N., Goltry,S., Lee,J., Yurke,B., Hughes,W.L. and Graugnard,E. (2017) Availability: a metric for nucleic acid strand displacement systems. *ACS Synth. Biol.*, **6**, 84–93.
24. Jiang,Y.S., Bhadra,S., Li,B. and Ellington,A.D. (2014) Mismatches improve the performance of strand-displacement nucleic Acid circuits. *Angew. Chem., Int. Ed.*, **53**, 1845–1848.
25. Lapteva,A.P., Sarraf,N. and Qian,L. (2022) DNA strand-displacement temporal logic circuits. *J. Am. Chem. Soc.*, **144**, 12443–12449.
26. Hong,F., Ma,D., Wu,K., Mina,L.A., Luiten,R.C., Liu,Y., Yan,H. and Green,A.A. (2020) Precise and programmable detection of mutations using ultraspecific riboregulators. *Cell*, **180**, 1018–1032.
27. Kim,P.B., Nelson,J.W. and Breaker,R.R. (2015) An ancient riboswitch class in bacteria regulates purine biosynthesis and one-carbon metabolism. *Mol. Cell*, **57**, 317–328.
28. Jones,C.P. and Ferré-D'Amaré,A.R. (2015) Recognition of the bacterial alarmone ZMP through long-distance association of two RNA subdomains. *Nat. Struct. Mol. Biol.*, **22**, 679–685.
29. Trausch,J.J., Marcano-Velázquez,J.G., Matyjasik,M.M. and Batey,R.T. (2015) Metal ion-mediated nucleobase recognition by the ZTP riboswitch. *Chem. Biol.*, **22**, 829–837.
30. Binas,O., Schamber,T. and Schwalbe,H. (2020) The conformational landscape of transcription intermediates involved in the regulation of the ZMP-sensing riboswitch from Thermosinus carboxydivorans. *Nucleic Acids Res.*, **48**, 6970–6979.
31. Dirks,R.M. and Pierce,N.A. (2003) A partition function algorithm for nucleic acid secondary structure including pseudoknots. *J. Comput. Chem.*, **24**, 1664–1677.
32. Chen,Y.-J., Liu,P., Nielsen,A.A.K., Brophy,J.A.N., Clancy,K., Peterson,T. and Voigt,C.A. (2013) Characterization of 582 natural and synthetic terminators and quantification of their design constraints. *Nat. Methods*, **10**, 659–664.
33. Larson,M.H., Greenleaf,W.J., Landick,R. and Block,S.M. (2008) Applied force reveals mechanistic and energetic details of transcription termination. *Cell*, **132**, 971–982.
34. Bushhouse,D.Z., Choi,E.K., Hertz,L.M. and Lucks,J.B. (2022) How does RNA fold dynamically?*J. Mol. Bio.*, **434**, 167665.
35. Cruz,V.E., Sekulski,K., Peddada,N., Sailer,C., Balasubramanian,S., Weirich,C.S., Stengel,F. and Erzberger,J.P. (2022) Sequence-specific remodeling of a topologically complex RNP substrate by Spb4. *Nat. Struct. Mol. Biol.*, **29**, 1228–1238.
36. Rodgers,M.L., Didychuk,A.L., Butcher,S.E., Brow,D.A. and Hoskins,A.A. (2016) A multi-step model for facilitated unwinding of the yeast U4/U6 RNA duplex. *Nucleic Acids Res.*, **44**, 10912–10928.
37. Landgraf,T., Völklein,A.E., Fürtig,B. and Schwalbe,H. (2022) The cotranscriptional folding landscape for two cyclic di-nucleotide-sensing riboswitches with highly homologous aptamer domains acting either as ON- or OFF-switches. *Nucleic Acids Res.*, **50**, 6639–6655.
38. Drogalis,L.K. and Batey,R.T. (2020) Requirements for efficient ligand-gated co-transcriptional switching in designed variants of the B. subtilis pbuE adenine-responsive riboswitch in E. coli. *PLoS One*, **15**, e0243155.
39. Breaker,R.R. (2011) Prospects for riboswitch discovery and analysis. *Mol. Cell*, **43**, 867–879.
40. Ceres,P., Trausch,J.J. and Batey,R.T. (2013) Engineering modular 'ON' RNA switches using biological components. *Nucleic Acids Res.*, **41**, 10449–10461.
41. Ceres,P., Garst,A.D., Marcano-Velázquez,J.G. and Batey,R.T. (2013) Modularity of select riboswitch expression platforms enables facile engineering of novel genetic regulatory devices. *ACS Synth. Biol*, **2**, 463–472.
42. Harbaugh,S.V., Silverman,A.D., Chushak,Y.G., Zimlich,K., Wolfe,M., Thavarajah,W., Jewett,M.C., Lucks,J.B. and Chávez,J.L. (2022) Engineering a synthetic dopamine-responsive riboswitch for *in vitro* biosensing. *ACS Synth. Biol.*, **11**, 2275–2283.